JOURNAL OF SOLID STATE CHEMISTRY 59, 42–53 (1985)

Nonstoichiometry, Cation Distribution, and Electrical Properties in Fe_3O_4–$CoFe_2O_4$ at High Temperature*

D. S. ERICKSON† AND T. O. MASON‡

Department of Materials Science and Engineering, Northwestern University, The Technological Institute, Evanston, Illinois 60201

Received September 10, 1984; in revised form January 2, 1985

Cation distributions in the system Fe_3O_4–$CoFe_2O_4$ from 600 to 1300°C were calculated from high-temperature thermopower measurements on oxygen-stoichiometric specimens. Behavior is virtually identical to that in the Fe_3O_4–$MgFe_2O_4$ system. Conductivity in $Co_xFe_{3-x}O_4$ ($x < 1$) obeys the relationship

$$\sigma = [de/(d + e)]T^{-1} \exp[14.3 - 1475\ T^{-1}(1 + 1.189x^2)],$$

where d and e are the octahedral Fe^{2+} and Fe^{3+} occupancies, respectively.

Introduction

This study was undertaken to determine the relationship between the cation distribution and electrical properties in Fe_3O_4–$CoFe_2O_4$ at high temperature (600–1300°C). The valence state and distribution of transition metal cations between sublattices in spinels is known to govern the electrical properties *in situ*, as well as the magnetic and electrical properties on cooling or quenching. This is of technological importance as cobalt is an important constituent of commercial magnetic ferrites. In addition, certain thermistor formulations involve cobalt and/or iron spinels (*1*). Electrochemical and photochemical applications involving cobalt ferrite electrodes are also conceivable (*2*). For such applications, a thorough understanding of the cation distribution, its temperature and/or time dependence, and its effect on the physical properties (e.g., electrical, magnetic) is essential.

Divalent cobalt behaves like divalent iron in the spinel lattice. The melting points of Fe_3O_4 and $CoFe_2O_4$ are quite similar (*3*). The diffusion coefficients of iron and cobalt in Fe_3O_4 are almost indistinguishable (*4*). The thermodynamic activity of Fe_3O_4 in the Fe_3O_4–$CoFe_2O_4$ solid solution is very nearly ideal (*5*). One goal of this study was to evaluate the influence, if any, of cobalt substitution upon the iron cation distribution thermodynamics. In a similar system, Fe_3O_4–$MgFe_2O_4$, a sizeable effect was observed (*6*).

Anomalies in the system Fe_3O_4–$CoFe_2O_4$ have been reported. In particular, Burriesci

* Based in part on an M.S. thesis by D. S. Erickson, May 1984.

† Now at Institute of Gas Technology, Chicago, Ill.

‡ To whom correspondence should be addressed.

0022-4596/85 $3.00

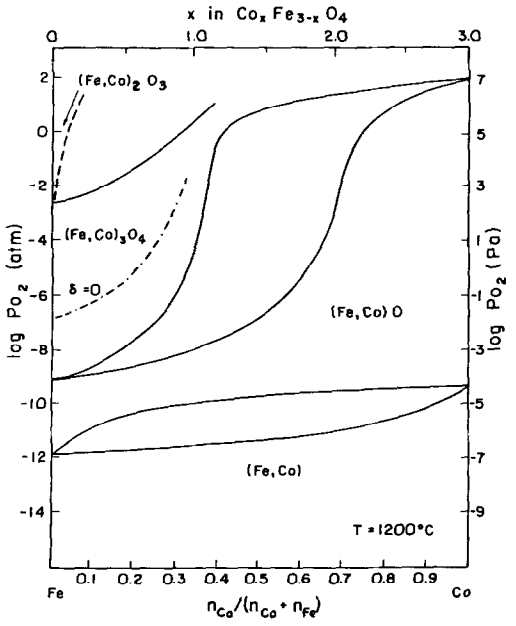

FIG. 1. The 1200°C phase diagram for the system Fe–Co–O. The dash-dot line gives the approximate conditions for oxygen stoichiometry in the spinel phase. This diagram is taken from Ref. (*9*).

et al. (*7*) recently demonstrated a marked Fe/Co surface segregation effect in cobalt ferrites. Yamada (*8*) observed large changes in the Seebeck coefficients of cobalt ferrite single crystals subjected to 24-hr high-temperature anneals. Similar effects were observed in the present study. It will be demonstrated, however, that these anomalies, attributable to surface cation segregation, can be avoided with special precautions.

Phase Equilibria, Valence States, and Cation Distribution in Fe_3O_4–Co_3O_4

Fe_3O_4–$CoFe_2O_4$ is a subsystem of the solid solution between Fe_3O_4 and Co_3O_4. A thorough review of the phase relationships in the system Fe–Co–O is given in Ref. (*9*). The 1200°C isotherm is shown in Fig. 1. The spinel phase equilibrates with the monoxide at low oxygen pressures and the sesquioxide at high oxygen pressures. It should be noted that equilibrium pressures exceed atmospheric for $x > 1$ in $Co_xFe_{3-x}O_4$ or $n_{Co}/(n_{Co} + n_{Fe}) > \frac{1}{3}$. This composition corresponds to $CoFe_2O_4$. The present study was limited to $x < 1$ and the solid solution between Fe_3O_4 and $CoFe_2O_4$.

The shape of the spinel region in Fig. 1 is indicative of the predominant valence states. At no oxygen pressure is the solid solution continuous from Fe_3O_4 to Co_3O_4. Instead, the spinel region can be divided into two distinct regions at $x = 1$ ($Co Fe_2O_4$). The spinel between $CoFe_2O_4$ and Co_3O_4 ($x \geq 1$) is stable over oxygen pressures where Fe^{3+} is the stable valence state in the Fe–O system (i.e., Fe_2O_3). This suggests that iron is predominantly trivalent in the range $1 < x < 3$. In contrast, the spinel between Fe_3O_4 and $CoFe_2O_4$ ($x < 1$) is stable over oxygen pressures where Co^{2+} is the stable valence state in the Co–O system (i.e., CoO) This suggests that cobalt is predominantly divalent in the range $0 < x < 1$ and that $Co_xFe_{3-x}O_4$ ($x \leq 1$) can be treated as a solid solution between Fe_3O_4 and $Co Fe_2O_4$.

The cation distribution in Fe_3O_4–Co_3O_4 has been estimated at one temperature by Pelton *et al.* (*10*) on the basis of phase boundary fitting techniques. The result, shown in Fig. 2, confirms the valence scheme outlined above. There is little or no

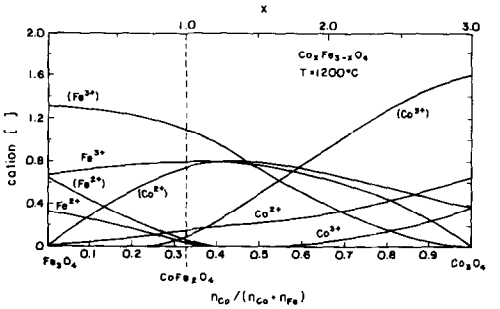

FIG. 2. The 1200°C cation distribution in $Co_xFe_{3-x}O_4$ after Ref. (*10*). Octahedral species are enclosed in parentheses.

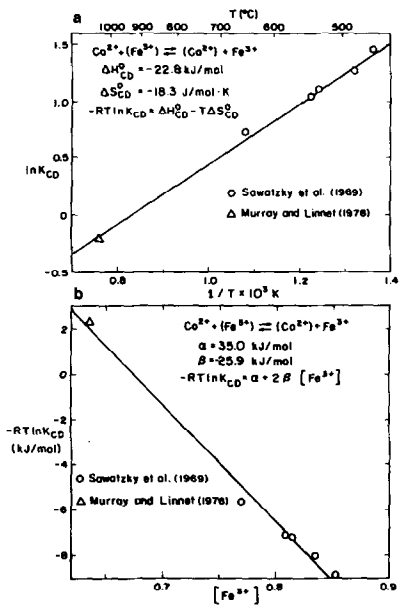

FIG. 3. Thermodynamic equilibrium plots for the cation distribution in $CoFe_2O_4$ after the models of (a) Navrotsky and Kleppa (Ref. (*15*)), and (b) O'Neill and Navrotsky (Ref. (*12*)). Data from Refs. (*13, 14*).

Fe^{2+} for compositions with $x > 1$ and little or no Co^{3+} for compositions with $x < 1$. Only in the vicinity of $CoFe_2O_4$ ($x = 1$) do all eight species need to be taken into account.

The cation distributions in the end members, Fe_3O_4 (*11, 12*) and $CoFe_2O_4$ (*13, 14*), are well established as a function of temperature. Two thermodynamic models have been employed to describe the temperature dependence of the equilibrium:

$$A^{2+} + (Fe^{3+}) \rightleftarrows (A^{2+}) + Fe^{3+};$$

$$K^{A}_{CD} = \frac{[(A^{2+})][Fe^{3+}]}{[A^{2+}][(Fe^{3+})]} \quad (1)$$

which describes the exchange of species between tetrahedral (open) and octahedral (enclosed in parentheses) sites. The divalent species A^{2+} is either Fe^{2+} or Co^{2+}. According to the model of Navrotsky and Kleppa (*15*), the temperature dependence of K^{A}_{CD} is given by

$$-RT \ln K^{A}_{CD} = \Delta H^{\circ}_{CD} - T\Delta S^{\circ}_{CD}, \quad (2)$$

where ΔH°_{CD} and ΔS°_{CD} are the enthalpy and nonconfigurational entropy of disorder. More recently, O'Neill and Navrotsky (*12, 16*) developed the expression

$$-RT \ln K^{A}_{CD} = \alpha + 2\beta[Fe^{3+}], \quad (3)$$

where $[Fe^{3+}]$ is the concentration of trivalent iron on the tetrahedral sublattice, β is a constant typically -20 ± 5 kJ/mole for $2^+/3^+$ spinels, and α is approximately the same magnitude, but with opposite sign. In Figs. 3a and b the data for $CoFe_2O_4$ are plotted according to Eqs. (2) and (3), respectively. Thermodynamic constants derived from these plots are given in Table I. Values for Fe_3O_4 (*11, 12*) and $MgFe_2O_4$ (*6*) are listed for comparison. With the exception of the α term, $CoFe_2O_4$ closely resembles Fe_3O_4. These thermodynamic parameters will be used to analyze the cation distributions in the Fe_3O_4–$CoFe_2O_4$ solid solution.

TABLE I

CATION DISTRIBUTION THERMODYNAMIC CONSTANTS

	Navrotsky/Kleppa model		O'Neill/Navrotsky model	
Spinel	ΔH° (kJ/mole)	ΔS° (J/mole · K)	α (kJ/mole)	β (kJ/mole)
Fe_3O_4	−23.0	−13.4	24.3	−23.0[a]
$CoFe_2O_4$	−22.8	−18.3	35.0	−25.9
$MgFe_2O_4$	−14.4	−4.0	17.4	−16.4

[a] Plus a nonconfigurational $\Delta S^{\circ} = -3.27$ J/mole · K.

Electrical Behavior and Nonstoichiometry in Fe_3O_4–$CoFe_2O_4$

An abrupt change in electrical properties at $x = 1$ ($CoFe_2O_4$) is well established (*17, 18*). This can be rationalized on the basis of the change in cation distribution at $x = 1$ in Fig. 2. For compositions with $x < 1$, small polaron hopping between Fe^{2+} and Fe^{3+} takes place. Conductivities are high ($>10^{-3}$ $(\Omega\ cm)^{-1}$) and activation energies are low ($\lesssim 0.2$ eV). Thermopower is negative, with absolute value decreasing away from the $CoFe_2O_4$ composition. For compositions with $x > 1$, however, no Fe^{2+} exists so that another conduction mechanism is operative. Conductivities are low ($<10^{-5}$ $(\Omega\ cm)^{-1}$) and activation energies are high (~ 0.5 eV). Thermopower is positive with large absolute value (400–800 μV/°K).

Numerous studies have been made of room temperature or slightly elevated temperature (RT – 1000 K) electrical properties in Fe_3O_4–$CoFe_2O_4$. These may be grouped according to the specimens employed—coarse-grained polycrystalline samples (*19–21*), ultrafine polycrystalline compacts (*18, 22, 23*), or single crystals (*8, 24*). The concensus of these studies is that conduction is via electron hopping between octahedral Fe^{2+} and Fe^{3+} with an activation energy in the range 0.1–0.2 eV. Conductivity decreases continuously from a maximum value of ~ 200 $(\Omega\ cm)^{-1}$ at $x = 0$ (Fe_3O_4) while thermopower, which is negative throughout, increases continuously in absolute value from Fe_3O_4 to $CoFe_2O_4$. Gillot (*23*) found that low-temperature (0–200°C) thermopower on stoichiometric, finely divided powder compacts fit the model developed by one of the authors (*25*). High-temperature electrical studies of the solid solution have not been reported.

In contrast, the high-temperature electrical properties of magnetite are well established (*11, 26*). Wu and Mason (*11*) derived the cation distribution versus temperature from single-crystal thermopower measurements. This information was later employed to analyze precise conductivity measurements on stoichiometric and nonstoichiometric single crystals (*26*). An octahedral small polaron conduction process was confirmed with an activation energy of 0.11 eV. Conductivity was insensitive to oxygen pressure variations over much of the stability range. From the variations at high oxygen pressure, vacancy formation constants were calculated which agreed well with those derived thermogravimetrically (*27*).

Nonstoichiometry in Fe_3O_4 solid solutions is due to iron interstitials at low oxygen pressures and iron vacancies at high oxygen pressures (*4, 27*). Dieckmann (*27*) gives the following abbreviated form for the deviation from stoichiometry (δ) in $Fe_{3-\delta}O_4$:

$$\delta = \frac{[Fe^{2+}]^3}{[Fe^{3+}]^2} \cdot K_V \cdot a_{O_2}^{2/3} - \frac{[Fe^{3+}]^2}{[Fe^{2+}]^3} \cdot K_I \cdot a_{O_2}^{-2/3}, \quad (4)$$

where K_V and K_I are the vacancy and interstitial constants, respectively, a_{O_2} is the oxygen activity, and $[Fe^{2+}]$ and $[Fe^{3+}]$ are the overall cation concentrations per lattice molecule. Following the procedure already employed for the Fe_3O_4–Fe_2TiO_4 solid solution (*28, 29*), Eq. (4) can be modified as follows:

$$\delta = \tfrac{1}{4}(1 - x)^3 \cdot K_V \cdot a_{O_2}^{2/3} - 4(1 - x)^{-3} \cdot K_I \cdot a_{O_2}^{-2/3}, \quad (5)$$

where x is the cobalt content in $Co_xFe_{3-x}O_4$. By setting $\delta = 0$, Eq. (5) can be solved at each value of x for the a_{O_2} corresponding to stoichiometry. Utilizing the defect constants supplied by Dieckmann (*27*), the stoichiometric 1200°C isotherm was calculated and superimposed on Fig. 1.

A questionable assumption in the procedure above is that the defect constants are

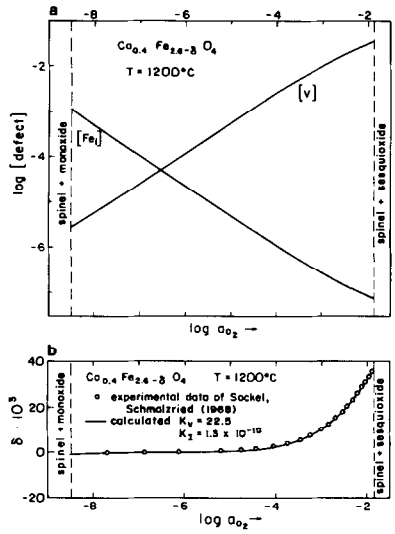

FIG. 4. Defect concentrations (a) and nonstoichiometry (b) in $Co_{0.4}Fe_{2.6}O_4$ based upon coulometric titration data (Ref. (*30*)). The curve is calculated according to Eq. (6) (see text).

independent of composition. To test this hypothesis, coulometric titration data of Sockel (*30*) at 1200°C for the composition $Co_{0.4}Fe_{2.6}O_4$ were analyzed following the procedure outlined in Ref. (*27*). Equation (4) must be modified as follows:

$$\delta = \frac{(1 - x - 3\delta)^3}{(2 + 2\delta)^2} \cdot K_V \cdot a_{O_2}^{2/3} - \frac{(2 + 2\delta)^2}{(1 - x - 3\delta)^3} \cdot K_I \cdot a_{O_2}^{-2/3}. \quad (6)$$

The Sockel data (*30*) and the curve calculated from Eq. (6) are shown in Fig. 4b. The individual defect concentrations are given in Fig. 4a. $Co_{0.4}Fe_{2.6}O_4$ is stoichiometric at $a_{O_2} = 10^{-6.5}$. This compares with $a_{O_2} = 10^{-5.9}$ calculated from Eq. (5) assuming the defect constants to be independent of composition. From Fig. 4 the defect constants at 1200°C in $Co_{0.4}Fe_{2.6}O_4$ are $K_V = 22.5$ and $K_I = 1.3 \times 10^{-10}$ as compared to $K_V = 20$ and $K_I = 8 \times 10^{-10}$ in Fe_3O_4 (*27*). Neither K_V nor K_I vary significantly with cobalt content, as assumed.

The effect of nonstoichiometry on conductivity and thermopower in $Co_xFe_{3-x}O_4$ can be explained with the aid of Fig. 4. Conductivity is proportional to the product, whereas thermopower is proportional to the ratio, of $[(Fe^{3+})]$ and $[(Fe^{2+})]$ on the octahedral sublattice (*25, 26*). Neither varies significantly with oxygen pressure as long as $|\delta| \leq 10^{-3}$. This condition encompasses a range of oxygen pressures extending from the phase boundary with monoxide up to 2.5 log a_{O_2} units from the phase boundary with sesquioxide. All measurements in the present study were made in this "plateau" region. Gas compositions were chosen to approximate the conditions of stoichiometry ($\delta = 0$) in Fig. 1.

Experimental

Polycrystalline specimens with the compositions $x = 0$, 0.2, 0.4, 0.6, and 0.8 in $Co_xFe_{3-x}O_4$ were sintered from powders prepared by resin intermediate method (*31*). Starting materials were reagent grade iron and cobalt nitrates, citric acid, and ethylene glycol. Solutions were gelled on a hot plate and subsequently calcined at 600–700°C overnight. The powders were then ground with mortar and pestle prior to reduction at 700°C for 2 hr under CO_2/CO reducing atmospheres. The gas compositions for this and all subsequent anneals were CO_2/CO = 100 for $x = 0$, 0.2, and 0.4, and CO_2/CO = 1000 for $x = 0.6$ and 0.8. Pellets were pressed and sintered to 90–96% theoretical density at 1300°C for 5 hr. X-Ray diffraction showed single-phase spinels at every composition. Quantitative chemical analysis confirmed the target compositions to within experimental uncertainty, and that no composition changes occurred during experiments. Rectangular bar specimens 1 × 1 × 15 mm were cut from sintered pellets with a diamond saw. The experimental furnace was a SiC-heated alumina muffle fur-

nace capable of ±1°C temperature control. CO_2/CO commercial premixtures were passed over the samples at ~1 linear cm/sec.

A description of the thermopower/conductivity apparatus is given elsewhere (*32*). The design given in Ref. (*32*) was slightly modified to position two Pt 6 Rh/Pt 30 Rh thermocouples on each side of the specimen. A small pressure was supplied by a spring to hold the sample in place. The sample holder was then positioned off the hot zone in the muffle furnace to achieve steady-state gradients of 15–20°C/cm along the specimen. With carefully matched thermocouples, this provided six thermal emf's and the corresponding six ΔT measurements for a thermopower plot. The four thermocouples were averaged to give the experimental temperature. Following the thermopower measurement, small microampere currents were passed in both directions between the outer thermocouples, and the emf average across the inner thermocouples was used to calculate sample conductivity. In this way, the thermal emf's were subtracted out. Conductivity was corrected for the percentage theoretical density. Thermopower was corrected for the Seebeck coefficient of the Pt 6 Rh common leads. Order of magnitude increases in a_{O_2} at high temperature (~1200°C) resulted in no significant changes in electrical properties. This was taken as confirmation of the stoichiometric plateau referred to previously.

Electrical measurements were made in ~100°C increments from 1300°C down to 600°C and then back to 1300°C. Readings were recorded after thermal voltages were stable (±2 μV) over 30 min. This was thought to indicate both cation distribution and oxygen equilibrium. At the lowest temperature, specimens were held overnight without significant changes in the readings. These observations were valid for the x = 0, 0.2, and 0.4 compositions only. At the x = 0.6 and 0.8 compositions, highly irreproducible results were obtained. It was felt that these were related to cation surface segregation, as documented in Ref. (*7*). This effect could be avoided by holding at each new temperature only long enough to obtain thermal equilibrium. Using this rapid measurement procedure, reproducible results were obtained for x = 0.6 and 0.8. Based upon kinetic studies in $MnFe_2O_4$ (*33*), it was felt that cation distribution (Fe *and* Co) should have been achieved even at the lowest temperature. The data support this contention (see Fig. 5). Original data are given in the Appendix.

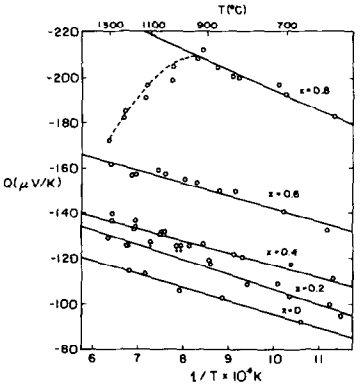

FIG. 5. Experimental thermopower in the system $Co_xFe_{3-x}O_4$.

Results and Cation Distribution Analysis

Thermopower results are plotted in Fig. 5. The choice of T^{-1} for abscissa is predicated upon the nearly linear dependence exhibited. This enables interpolation and extrapolation to other temperatures than those where actual measurements were made. The data are virtually identical to those in the Fe_3O_4–$MgFe_2O_4$ system (*6*), as expected, except for the downturn at high temperature for x = 0.8. This anomaly will be addressed in the following discussion.

It is interesting to note that the thermopower data for x = 0 agree with our earlier

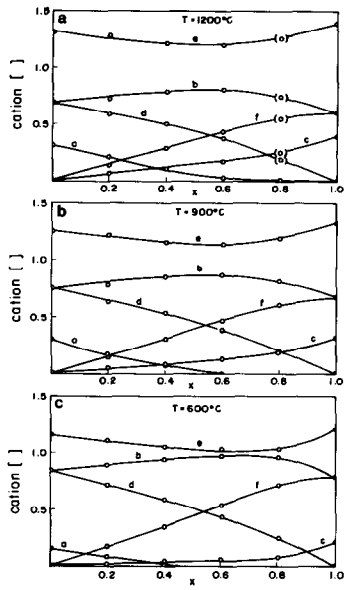

FIG. 6. Calculated cation distributions in the system Fe_3O_4–$CoFe_2O_4$ at (a) 1200°C, (b) 900°C, and (c) 600°C. Points for $x = 0.8$ at 1200°C based upon extrapolated thermoelectric coefficients (see Fig. 5).

single-crystal studies (*11*) to within 3–4 μV/K. Likewise, the conductivity data for $x = 0$ agree with our earlier single crystal values (*26*) to within 8%. This was thought to be a good test of the influence of polycrystallinity on the electrical properties.

The procedure for calculating the cation distribution from the thermopower data is outlined in Ref. (*6*). Site, charge, and mass balance equations are combined with the equilibria represented by Eq. (1) to solve for the site occupancies, a–f, per lattice molecule:

$$Fe_a^{2+}Fe_b^{3+}Co_c^{2+}(Fe_d^{2+}Fe_e^{3+}Co_f^{2+})O_4. \quad (7)$$

This results in the relationship

$$K_{CD}^{Co} = \frac{b\left(b - \dfrac{2-b}{q}\right)}{(2-b)\left(x - b + \dfrac{2-b}{q}\right)}, \quad (8)$$

where x is the cobalt concentration in $Co_xFe_{3-x}O_4$, b is the tetrahedral Fe^{3+} concentration per lattice molecule, and q is the octahedral valence ratio:

$$q = e/d = \tfrac{1}{2}\exp(-Qe/k). \quad (9)$$

Although the thermopower, Q, uniquely defines q, a value of K_{CD}^{Co} is still required to solve Eq. (8) for b and, therefore, the overall cation distribution. As mentioned previously, no data are available for K_{CD}^{Co} in the solid solution, so Eqs. (2) or (3) were used, employing the thermodynamic factors for $CoFe_2O_4$ in Fig. 3. The results were virtually identical whether $K_{CD}^{Co} \neq f(x)$ (Eq. (2)) or $-RT \ln K_{CD}^{Co} = \alpha + 2\beta(b)$ (Eq. (3)) was employed. The latter case results are displayed in Fig. 6 for 1200, 900, and 600°C. It can be seen that $K_{CD}^{Fe} = (bd/ae)$ changes dramatically across the solid solution,[1] as it did in the system Fe_3O_4–$MgFe_2O_4$ (*6*). This suggests that the O'Neill/Navrotsky model (Eq. (3)) is more appropriate.

The cation distributions in Fig. 6 are consistent with the findings of previous workers. The basic features are the same as in the 1200°C distribution for $x \leq 1$ of Pelton and co-workers (*10*) in Fig. 2, with the exception of the tetrahedral Fe^{2+} population, which declines more rapidly with x in our study. Franke and Rosenberg (*34, 35*) performed Mössbauer spectroscopy on cobalt ferrites air-quenched from 1200 to 1400°C. They obtained a reasonable fit to their octahedral site intensities by assuming a random mixture of inverse Fe_3O_4 and 24% disordered $CoFe_2O_4$. This would correspond to somewhere between our 600 and 900°C distributions, allowing for the complete inversion of iron during quenching. Although kinetic studies are not available for cobalt redistribution, practical experience suggests that air cooling would result in significantly less cobalt disorder than achieved by Murray and Linnert (*14*) in water quenching from 1050°C ($[Fe^{3+}] = 0.365$). The co-

[1] Due to the fact that $a = [Fe^{2+}] \rightarrow 0$.

balt distribution in the study of Franke and Rosenberg would, therefore, correspond to a lower temperature than 1050°C.

Two studies (*7, 20*) suggest that the saturation magnetization in Fe_3O_4–$CoFe_2O_4$ is composition independent when air quenching is employed. This is consistent with the cation distributions in Fig. 6. It can be seen that the cobalt site occupancies are nearly linear functions of x, regardless of temperature. Assuming total inversion of iron on air quenching ($a = [Fe^{2+}] \rightarrow 0$) the resulting distribution would be

$$Fe^{3+}_{1-xc_0}Co^{2+}_{1-xc_0}(Fe^{2+}_{1-x}Fe^{3+}_{1+xc_0}Co^{2+}_{x(1-xc_0)})O_4, \quad (10)$$

where c_0 is the degree of disorder in $CoFe_2O_4$. Assuming colinear ferrimagnetic ordering, this would correspond to a saturation magnetization:

$$M_s = 4 - x(1 - 4c_0) \quad (11)$$

in Bohr magnetons. It follows that for 25% cobalt disorder ($c_0 = 0.25$), the saturation magnetization would be composition independent. This is consistent with the disorder found in air-quenched Fe_3O_4–$CoFe_2O_4$ (*34, 35*) and should correspond to an equilibrium temperature of approximately 700°C.

The 1200°C magnetite activity in the solid solution Fe_3O_4–Co_3O_4 was reported by Aukrust and Muan (*5*). Following the same procedure as for Fe_3O_4–$MgFe_2O_4$ (*6*), the free energy of mixing (ΔG^m) can be calculated from the 1200°C cation distribution in Fig. 6 using the relation

$$\Delta G^m \simeq -T\,\Delta S_c, \quad (12)$$

where the configurational entropy is given by

$$S_c = -R \sum_s \sum_i b^s n_i^s \ln n_i^s$$

which sums over both species (i) and sites (s). Here n_i^s is a site fraction and b^s is the number of sites per lattice molecule (i.e., $b^{tet} = 1$, $b^{oct} = 2$). We have neglected excess enthalpy terms because there is negligible size mismatch between Co^{2+} and iron, and there is very little variation in $b = [Fe^{3+}]$ with composition. See Ref. (*16*) for a discussion of this procedure. Fe_3O_4 activities were calculated from the tangents to the ΔG^m curves. The results are compared with the curve reported by Aukrust and Muan (*5*) in Fig. 7. Agreement is quite satisfactory over $0 \leq x \leq 0.8$, however, a discrepancy occurs in the vicinity of $CoFe_2O_4$. This may be associated with our model which assumes no Co^{3+} in the Fe_3O_4–$CoFe_2O_4$ system and forces the activity of Fe_3O_4 to zero at $x = 1$. Aukrust and Muan (*5*) detected a small magnetite activity in $CoFe_2O_4$. More recent activity measurements in Fe_3O_4–$CoFe_2O_4$ (*36*) detected a slight negative deviation from ideality from $x = 0.6$ to $x = 1$. These samples were equilibrated with sesquioxide, however, and should have smaller Fe_3O_4 activities due to oxidation.

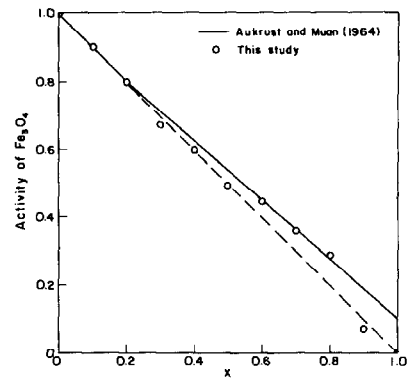

FIG. 7. Calculated vs measured (Ref. (*5*)) Fe_3O_4 activities in the Fe_3O_4–$CoFe_2O_4$ solid solution.

Conductivity Analysis

Small polaron conductivity (σ) obeys the following relationship (*26, 37, 38*)

$$\sigma = \frac{gNc'(1 - c')e^2a^2\nu_0}{kT} \exp\left(-\frac{E_H}{kT}\right), \quad (13)$$

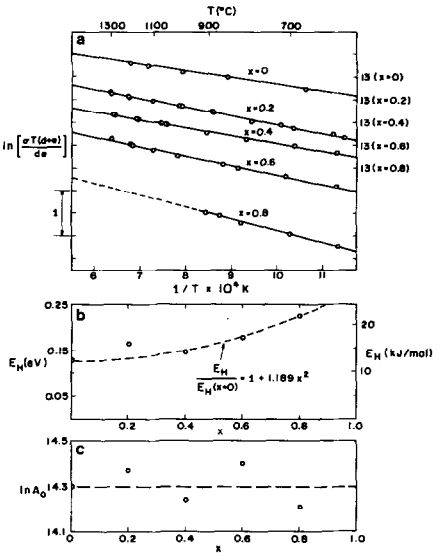

FIG. 8. Conductivity analysis in $Co_xFe_{3-x}O_4$ based upon small polaron theory. (a) Arrhenius plot, (b) activation energies, (c) preexponential factors.

where g is a geometrical factor, N is the density (cm^{-3}) of conducting sites, a fraction c' occupied by carriers, and a fraction $(1 - c')$ of available sites, a is the jump distance (cm), ν_0 is the lattice vibrational frequency responsible for conduction (sec^{-1}), E_H is the activation energy for hopping, and the remaining terms (e, k, T) have their usual meanings. For an octahedral small polaron process, $g = 1$ and:

$$N = N_{sp}(d + e), \tag{14}$$

where N_{sp} is the density of spinel lattice molecules (cm^{-3}), and d and e refer to the Fe^{2+} and Fe^{3+} octahedral occupancies (see Eq. (7)). It follows that $c' = d/(d + e)$ and $(1 - c') = e/(d + e)$. Substituting into and rearranging Eq. (13) results in the expression

$$\ln\left[\frac{\sigma T(d+e)}{de}\right] = \ln\left[\frac{N_{sp}e^2a^2\nu_0}{k}\right] - \frac{E_H}{kT} = \ln A_0 - \frac{E_H}{kT}. \tag{15}$$

It follows that an Arrhenius plot of $\ln[\sigma T(d + e)/de]$ vs T^{-1} should have a slope of $-E_H/k$ and an intercept of $\ln A_0$. Values for $(d + e)/de$ were obtained from the thermoelectric coefficients as outlined above (see Fig. 6). The conductivity results are plotted as required in Fig. 8a. Note that the ordinate scale has been shifted for each composition so that the data do not superimpose. The activation energies (Fig. 8b) and preexponential factors (Fig. 8c) do not change very much with composition. The composition independence of A_0 indicates that ν_0 is not a function of composition. Since the lattice parameter is constant across the Fe_3O_4 solid solution, N_{sp} and a will also be constant. The value for ν_0 calculated from A_0 is 7.5×10^{13} sec^{-1}, which compares favorably with 6.7×10^{13} sec^{-1} reported for single-crystal Fe_3O_4 (*26*). Although microcracks and grain boundaries can significantly alter electrical conductivity in ceramics, the agreement between the polycrystalline results in the present study and previous single-crystal measurements provides some measure of confidence that bulk properties were being measured.

A general expression can be derived for the high-temperature conductivity in Fe_3O_4–$CoFe_2O_4$. In Fig. 8b the activation energy was fit to the relationship

$$E_H = E_H(x = 0)[1 + 1.189x^2]. \tag{16}$$

The $x = 0.2$ value was not included in the fitting. In other ferrospinels, monotonic increases in E_H with composition have been observed (*6, 38*). The $x = 0.4$, 0.6, and 0.8 data fit nicely in Eq. (16). Substituting Eq. (16) into Eq. (15) and rearranging, the resulting conductivity expression is

$$\sigma = [de/(d + e)]T^{-1} \exp[14.3 - 1475T^{-1}(1 + 1.189x^2)]. \tag{17}$$

The term $de/(d + e)$ must be calculated from the thermopower or from the data given in Fig. 6. With the exception of $x = 0.2$, an excellent fit to the experimental conductivity is achieved. It was felt that the x

= 0.2 conductivity was lower than it should have been, possibly due to the microcracking mentioned previously. As an alternative to the lengthy procedure of calculating the cation distribution from the thermopower, the following simplification can be made:

$$\frac{de}{d+e} \approx \frac{d_0(1-x)e_0}{d_0(1-x)+e_0}, \qquad (18)$$

where d_0 and e_0 represent the octahedral Fe^{2+} and Fe^{3+} occupancies in Fe_3O_4, which can be calculated according to the procedure given in Ref. (*11*). This assumes a linear variation of $d = [(Fe^{2+})]$ with composition.

Discussion

The octahedral small polaron model adequately explains electrical behavior for $0 \leq x < 0.8$ in $Co_xFe_{3-x}O_4$. It cannot, however, account for the downturn in thermopower at temperatures above 900°C for the $x = 0.8$ specimen (see Fig. 5). It is interesting that the discrepancy between calculated and measured Fe_3O_4 activities occurs at approximately the same composition (see Fig. 7). This suggests that the presence of Co^{3+} could be accountable for both anomalies. It is well documented that conduction changes from n to p at $x = 1$ ($CoFe_2O_4$). Perhaps the p-type process is favored at elevated temperatures. Additional studies would be necessary to resolve this issue.

The irreproducibilities after lengthy anneals of the $x = 0.6$ and $x = 0.8$ compositions were attributed to surface cation segregation. The interesting aspect of these anomalies is that conductivity was unaffected whereas thermopower was altered noticeably. This can be explained as follows. Iron preferentially segregates to the surface, according to Burriesci *et al.* (*7*). This would result in a higher conductivity surface layer with a thermopower shifted toward that of Fe_3O_4. But since E_H is only a weak function of x, and the preexponential factors are constants for $Co_xFe_{3-x}O_4$, merely redistributing Fe and Co should result in negligible overall changes in conductivity. The thermopower, however, would be given by

$$Q_{tot} = \frac{Q_s\sigma_s + Q_i\sigma_i}{\sigma_{tot}}, \qquad (19)$$

where s = surface and i = interior. Although σ_{tot} remains approximately constant, Q_{tot} will depend upon the relative conductivities of surface and interior.

Finally, it should be mentioned that K_{CD}^{Fe} is a strong function of composition in Fe_3O_4–$CoFe_2O_4$. This can be demonstrated from the fact that $a = [Fe^{2+}]$ goes to zero at increasingly smaller values of x as temperature decreases (see Fig. 6). This is particularly surprising when one considers that Co^{2+} behaves so similarly to Fe^{2+} in the spinel lattice. The effect of cobalt on K_{CD}^{Fe} cannot be explained on the basis of the O'Neill/Navrotsky (*12, 16*) model. For a discussion of this phenomenon see Ref. (*39*).

Acknowledgments

The authors gratefully acknowledge the support of the National Science Foundation under Grant DMR-8106492. Specimens were prepared in the Ceramics Facility of Northwestern University's Materials Research Center, supported in part under the NSF-MRL program (Grant DMR82-16972). The authors are grateful to S. E. Dorris for helpful discussions.

References

1. H. B. Sachse, "Semiconducting Temperature Sensors and Their Application," Wiley, New York (1975).
2. M. D. Archer, G. C. Morris, and G. K. Yim, *J. Electroanal. Chem. Interfacial Electrochem.* **118,** 89 (1981).
3. D. P. Masse and A. Muan, *J. Amer. Ceram. Soc.* **48,** 467 (1965).
4. R. Dieckmann, T. O. Mason, J. D. Hodge, and H. Schmalzried, *Ber. Bunsenges. Phys. Chem.* **82,** 778 (1978).

Appendix

Raw Conductivity Data for $Co_xFe_{3-x}O_4$ (All Data in $(\Omega\text{-cm})^{-1}$)

$x = 0$		$x = 0.2$		$x = 0.4$		$x = 0.6$		$x = 0.8$	
T(°C)	σ	T(°C)	σ	T(°C)	σ	T(°C)	σ	T(°C)	σ
670	174.0	599	95.0	611	96.8	611	62.3	609	17.9
857	181.8	618	99.8	690	102.5	709	68.5	701	20.1
990	183.8	693	103.3	690	100.3	821	71.6	812	22.5
1125	183.3	718	108.7	800	104.5	860	75.6	870	24.8
1200	183.7	788	108.2	909	108.6	1006	79.0	912	24.7
		890	117.4	909	108.9	1096	81.3	1018	26.9
		895	119.4	1045	113.5	1098	81.4	1019	28.5
		990	125.9	1048	112.4	1101	82.3	1120	30.0
		1002	125.4	1065	114.2	1189	84.2	1124	30.6
		1102	127.3	1165	116.9	1201	85.8	1217	32.8
		1103	127.2	1168	115.2	1296	91.5	1225	33.3
		1204	125.8	1170	116.6	1298	89.3	1301	35.6
		1211	125.9	1282	118.5				
		1300	128.6	1283	117.7				
		1305	128.7						

Raw Thermopower Data for $Co_xFe_{3-x}O_4$ (All Data in $(\Omega V/K)$)

$x = 0.2$		$x = 0.4$		$x = 0.6$		$x = 0.8$	
T(°C)	Q	T(°C)	Q	T(°C)	Q	T(°C)	Q
599	− 98	611	−111	621	−132	609	−183
694	−103	690	−117	705	−141	701	−193
788	−111	800	−120	819	−150	812	−200
895	−115	954	−125	933	−153	870	−204
999	−119	1047	−130	1101	−157	931	−208
1102	−123	1164	−134	1201	−159	1019	−205
1211	−126	1283	−137	1298	−162	1124	−191
1300	−130					1224	−182
						1301	−172

5. E. AUKRUST AND A. MUAN, *Trans. AIME* **230,** 1395 (1964).
6. A. TRESTMAN-MATTS, S. E. DORRIS, AND T. O. MASON, *J. Amer. Ceram. Soc.* **67,** 69 (1984).
7. N. BURRIESCI, F. GARBASSI, AND S. PIZZINI, *J. Magn. Magn. Mater.* **7,** 52 (1978).
8. T. YAMADA, *J. Phys. Soc. Jpn.* **35,** 130 (1973).
9. J. STICHER AND H. SCHMALZRIED, "The Geometrical Representation of Thermodynamic Equilibria in Multicomponent Systems Based on Iron," Rep. Inst. Theor. Met. Phys. Chem., Tech. Univ. Clausthal, Fed. Rep. Ger. (May, 1975).
10. A. D. PELTON, H. SCHMALZRIED, AND J. STICHER, *Ber. Bunsenges. Phys. Chem.* **83,** 241 (1979).
11. C. C. WU AND T. O. MASON, *J. Amer. Ceram. Soc.* **64,** 520 (1981).
12. H. S. C. O'NEILL AND A. NAVROTSKY, *Amer. Mineral.* **68,** 181 (1983).
13. G. A. SAWATZKY, F. VANDERWOUDE, AND A. H. MORRISH, *Phys. Rev.* **187,** 747 (1969).
14. P. J. MURRAY AND J. W. LINNETT, *J. Phys. Chem. Solids* **37,** 1041 (1976).
15. A. NAVROTSKY AND O. J. KLEPPA, *J. Inorg. Nucl. Chem.* **29,** 2701 (1967).

16. H. S. C. O'Neill and A. Navrotsky, *Amer. Mineral.* **69,** 733 (1984).
17. G. H. Jonker, *J. Phys. Chem. Solids* **9,** 165 (1959).
18. B. Gillot and F. Jemmali, *Phys. Status Solidi A* **76,** 601 (1983).
19. S. Iida, H. Sekizawa, and Y. Aiyama, *J. Phys. Soc. Jpn.* **13,** 58 (1958).
20. Y. Kumashiro, *J. Electrochem. Soc. Jpn.* **35,** 210 (1967).
21. C. Constantin and M. Rosenberg, *Solid State Commun.* **9,** 675 (1971).
22. A. C. C. Tseung and J. R. Goldstein, *J. Mater. Sci.* **7,** 1383 (1972).
23. B. Gillot, *Phys. Status Solidi A* **69,** 719 (1982).
24. S. G. Kimmet and R. P. Poplawsky, *Mater. Sci. Eng.* **16,** 265 (1974).
25. C. C. Wu, S. Kumarakrishnan, and T. O. Mason, *J. Solid State Chem.* **37,** 144 (1981).
26. R. Dieckmann, C. A. Witt, and T. O. Mason, *Ber. Bunsenges. Phys. Chem.* **87,** 495 (1983).
27. R. Dieckmann, *Ber. Bunsenges. Phys. Chem.* **86,** 112 (1982).
28. R. Aragon and R. H. McCallister, *Phys. Chem. Miner.* **8,** 112 (1982).
29. A. Trestman-Matts, S. E. Dorris, S. Kumarakrishnan, and T. O. Mason, *J. Amer. Ceram. Soc.* **66,** 829 (1983).
30. H.-G. Sockel and H. Schmalzried, *Ber. Bunsenges. Phys. Chem.* **72,** 745 (1968).
31. P. Pechini, U.S. Patent 3,330,697, July 11, 1967.
32. A. Trestman-Matts, S. E. Dorris, and T. O. Mason, *J. Amer. Ceram. Soc.* **66,** 589 (1983).
33. Z. Jirak and S. Vratislav, *Czech. J. Phys. Sect. B.* **24,** 642 (1974).
34. H. Franke and M. Rosenberg, *J. Magn. Magn. Mater.* **4,** 186 (1977).
35. H. Franke and M. Rosenberg, *Physica B* **86–88,** 965 (1977).
36. I. Katayama, T. Matsuda, and Z. Kozuka, *Nippon Kinzoku Gakkaishi* **47,** 858 (1983).
37. H. L. Tuller and A. S. Nowick, *J. Phys. Chem. Solids* **38,** 859 (1977).
38. T. O. Mason and H. K. Bowen, *J. Amer. Ceram. Soc.* **64,** 237 (1981).
39. S. E. Dorris and T. O. Mason, "Electrical Characterization of High Temperature Site Occupancies in Spinel Ferrites and Manganites," Fourth International Conf. on Ferrites, Oct. 31–Nov. 2, 1984.